Spatial Statistics 18 (2016) 221–233

Contents lists available at ScienceDirect

Spatial Statistics

journal homepage: www.elsevier.com/locate/spasta

The impact of averaging methods on the trend analysis of the Antarctic sea ice extent and perimeter

Xi Zhao [a], Lei Xu [b], Alfred Stein [c], Xiaoping Pang [a,*]

[a] Chinese Antarctic Center of Surveying and Mapping, Wuhan University, Wuhan 430079, China
[b] School of Resource and Environmental Science, Wuhan University, Wuhan 430079, China
[c] Faculty of Geo-Information Science and Earth Observation, Twente University, The Netherlands

ARTICLE INFO

Article history:
Received 30 December 2015
Accepted 6 April 2016
Available online 20 April 2016

Keywords:
Sea ice
Random set
Trend
Extent
Averaging method
Antarctic

ABSTRACT

To estimate the long-term trends in changes for the Antarctic sea ice, daily extents of sea ice were integrated to monthly averages. Different integration methods, however, result in monthly ice extents with inconsistent boundaries that may have further impact on the estimated trend rates. We used random sets to model the sea ice extent and we compared five averaging methods to derive the monthly expectation from a set of daily ice extents and examined their differences in the trend analysis. The Antarctic sea ice extent exhibited consistent statistically significant upward trends for the period November 1978–December 2014 at a rate of approximately $24 \pm 2.3 \times 10^3$ km^{2}yr^{-1}. The trends in the sea ice perimeter, however, do not agree and its estimation is more sensitive to the averaging methods. Large gaps among monthly sea ice boundaries occurred in the regions where sea ice retreated or expanded dramatically in a single month, especially in the Weddell Sea and the Indian Ocean during the month of December. The study showed that more attention should be given to these regions during periods that the daily sea ice experiences more notable dynamics. We finally commented that the median set can serve as a widely applicable method for both ice extent and perimeter and that the Vorob'ev expectation is appropriate only for the extent estimation.

* Corresponding author.
E-mail address: pxp@whu.edu.cn (X. Pang).

http://dx.doi.org/10.1016/j.spasta.2016.04.002
2211-6753/

1. Introduction

Sea ice is an integral component of the climate system that both affects and also reflects changes in other climate components (Massom and Stammerjohn, 2010). Because sea ice in the polar region is sensitive to climate change on a global scale, trends in its current dynamics and changes are of particular interest to scientific committees and governments (Simmonds, 2015). Satellite passive-microwave images have been used to produce sea ice concentration data, i.e., the percentage of areal ice coverage, since 1978. These have been used to measure the boundaries and areas of sea ice regions, thus providing a daily monitoring of Arctic and Antarctic sea ice for almost four decades. The Intergovernmental Panel on Climate Change Fourth Assessment Report (IPCC AR4) and Fifth Assessment Report (IPCC AR5) show a rapidly diminishing ice extent in the Arctic but an opposite trend in Antarctic. Interestingly, the IPCC AR5 reported that the observed Antarctic sea ice extent expands at a statistically significant rate of $16.5 \pm 3.5 \times 10^3$ km^2 yr^{-1} (IPCC, 2013). This is in substantial contrast with the small and statistically insignificant rate of $5.6 \pm 9.2 \times 10^3$ km^2 yr^{-1} reported in IPCC AR4 (IPCC, 2007).

To calculate the change rate of sea ice, we used satellite passive-microwave images. First, the ice concentration data (proportion of ice area in a pixel) was derived from passive microwave measurements. The sea ice extent is defined as the area of ice that has an ice concentration of no less than 15%. Next, the daily ice extents are averaged to determine monthly mean values. On the basis of those values, monthly deviations are derived and a linear regression model is applied to determine the rate (Parkinson and Cavalieri, 2012). This is currently a standard practice that started in Parkinson et al. (1999) and has been followed by subsequent works (Parkinson and Cavalieri, 2012; Cavalieri and Parkinson, 2008, 2012). During this process, uncertainties from sensor transitions, processing method updates and the addition of new data sources can all influence the final result (Eisenman et al., 2014; Cavalieri et al., 2012). For example, in using passive microwave measurements to determine ice concentrations, there are more than thirty different algorithms that can be selected, with a portion even having different versions (Ivanova et al., 2015). Eisenman et al. (2014) found that a substantial change in the long-term trend was caused by a change in the intercalibration across a 1991 sensor transition when the Bootstrap data set was updated to Version 2 in 2007. Ivanova et al. (2015) subsequently presented the results of an extensive inter-comparison algorithm to find the optimal SIC algorithm in which a climate time series has a low sensitivity to error sources. Unfortunately, their conclusions showed that no one single algorithm is superior as concerns all criteria. Additionally, for the uncertainties associated with image processing, the choice of a statistical method utilized as the final step can also introduce a large variation in trend analyses. By treating the daily ice extent as a random variable, calculation of an arithmetic monthly mean value based upon the daily extent data is a basic way to determine the monthly extent. In this common practice, however, the spatial information on the distribution of the sea ice is missing and we do not even know where the boundary of the monthly sea ice is located. Moreover, the arithmetic mean is not the only way to summarize the daily data and we may ask how other averaging methods will impact the trend estimation.

Averaging is a basic statistical concept, but it becomes fairly complicated for random sets and for random shapes in a non-linear space. A random set is a generalization of a random variable, whose values are sets (Molchanov, 2005). Because they provide a foundation for set-theoretic statistical approaches, random sets have been successfully employed for developing image averaging methods as well as for the study of randomly varying geometrical shapes (Friel and Molchanov, 1999; Stoyan and Stoyan, 1994). In this study, we first treat the spatial extents of daily sea ice in a single month as a set of objects with randomly varying shapes and then derive the monthly average extent as the expectation of the random set. There is no universal definition of the expectation for random sets; however, some definitions highlight certain features in particular contexts (Molchanov, 1998). The Vorob'ev expectation has been used to extract natural objects with vague boundaries in wetland areas (Zhao et al., 2010) and also to simulate the fire spread with irregular boundaries in a forest (Vorob'ov, 1996). Expectations based on various distance functions were applied to determine an average shape of characters from the collection of scanned newspaper images (Baddeley and Molchanov, 1998; Jankowski and Stanberry, 2010). A Fréchet expectation based on the Hausdorff distance was successfully utilized to identify the mean of geometrically constrained traffic island polygons (Zhou, 2014).

The aim of this study was to test the impact of using different averaging methods for evaluation of the long-term trends of sea ice extent and perimeter. To this end, we implemented several expectations of random sets to derive the spatial boundaries of monthly sea ice extents and compared their sizes, perimeters and spatial ranges. We intended to determine the times at which the biggest variations occurred and the regions where large gaps occurred based on different monthly extents. Long-term trends were further estimated and compared using the different averaging methods. We evaluated the impact of averaging methods on the trend analysis based upon differences in the change rates and their statistical significance. Finally, the features of each method were discussed and the appropriate method has been recommended for sea ice analysis.

2. Methods and data

2.1. Image data

The sea ice concentration data sets considered in this study are derived using passive microwave measurements from the Scanning Multichannel Microwave Radiometer (SMMR) on the Nimbus-7 satellite, from the Special Sensor Microwave/Imager (SSM/I) sensors on the Defense Meteorological Satellite Program's (DMSP) -F8, -F11, and -F13 satellites and from the Special Sensor Microwave Imager/Sounder (SSMIS) onboard DMSP-F17. The data were processed using the Bootstrap Algorithm (Version 2) at NASA Goddard Space Flight Center and distributed by the National Snow and Ice Data Center (Comiso, 2000, updated2015). We chose the Bootstrap algorithm for this study, being a widely used ice concentration product, also providing the database for the IPCC reports. Daily (every other day prior to July 1987) data gridded on an SSM/I polar stereographic grid (25 $\times$ 25 km) were selected for the south polar regions for the period of 1 November 1978–31 December 2014.

2.2. Monthly mean processing

During image processing, the sea ice extent is identified by including grid cells with ice concentration above 15% to avoid wind roughing and other weather filtering issues near the ice edge. Explanation for the 15% threshold can be found in Worby and Comiso (2004). The sea ice perimeter is extracted as the boundary between the sea ice and the ocean. In a standard convention, the monthly mean is the arithmetic average of the daily extents. This value only has attribute information and cannot be mapped spatially. In this study, we applied five methods to extract the spatial extent of monthly means in different ways. We then calculated the area and perimeter of the monthly extents based on the figures in two-dimensional space.

A straightforward way to envision this process is to first compute the monthly averaged ice concentration fields from the daily ice concentration data and then identify the monthly ice extent (denoted by M_A) by including grid cells with ice concentrations above 15%. A previous study indicated that this calculation can result in bias associated with the merging of temporal and spatial averages (Eisenman et al., 2014). We kept this method in our study for comparison with results from other methods.

By constructing random sets for each calendar month, we aimed to identify some features, such as the area of a region, which can be described as a random variable in a linear space. Several methods of defining the means of random sets are based upon the inverse images of the expectations of these features. Widely accepted definitions include the Aumann expectation, the Vorob'ev expectation, the Radius-vector expectation, the Fréchet expectation and the Distance average (Molchanov, 1998; Friel and Molchanov, 1999; Stoyan, 1997). The choice of a particular definition depends upon the aim of the specific application. In this image analysis study, we selected the Vorob'ev expectation (denoted as M_V), an oriented Distance average (denoted as M_O) and a Hausdorff distance-based Fréchet expectation (denoted as M_H) to determine the monthly mean ice extent.

The daily ice extent is used to construct a random set for month t, denoted as Γ^t, representing the stochastic shape of the ice extent in that month. The covering function, also called the one-point coverage function (Stoyan and Stoyan, 1994), serves to characterize the distribution of the random set

Γ. The covering function $Pr_\Gamma(x)$ at pixel x is defined as $P(\Gamma \cap \{x\} \neq \emptyset) = P(x \in \Gamma)$. It is estimated as:

$$\hat{P}r_\Gamma(x) = \frac{1}{n}\sum_{i=1}^{n} I_{O_i}(x)$$

where O_i is the realization of Γ, e.g., the daily ice extent, and $I_{O_i}(x)$ is the indicator function of $O_i(x)$. Pixels with $Pr_\Gamma(x) \geq p$ constitute a p-level set of Γ. The support set (0-level set) and core set (1-level set) delineate the extent of the possible maximum ice area and the definite sea ice area in a month, respectively. The median set of Γ^t is the 0.5-level set (denoted as M_M) that delineates the regions that sea ice is covering for half of the time period.

The Vorob'ev mean of random set (M_V) is estimated by first determining the expectation of the covering function $EA(\Gamma) = \int_{R^2} Pr_\Gamma(x)dx$ and then determining a p-level set that has an area equal to $EA(\Gamma)$:

$$M_V = \{x \in R^2,\ 0 \leq p_m \leq 1 :\ Pr_\Gamma(x) \geq p_m\}$$

where p_m is determined for the set M_V that has the area $EA(\Gamma)$. If p_m is not unique, then the infimum of all such p_ms can be used. If $p_m = 0.5$, then M_V and M_M are identical. In the sea ice case, if the probability distribution of daily extents within a month is approximately symmetrical, M_V and M_M are likely to be equal.

The Vorob'ev mean M_V is determined by the covering function, which is the average of the indicator functions. M_O replaces the indicator functions with oriented distance functions and characterizes the expectation of the random set using the distance average (Baddeley and Molchanov, 1998; Jankowski and Stanberry, 2010). M_O is then defined as the pixels with positive average oriented distance function $\hat{b}_\Gamma(x)$:

$$M_O = \{x \in R^2 :\ \hat{b}_\Gamma(x) \geq 0\}.$$

The average oriented distance function of Γ at pixel x is denoted as $\hat{b}_\Gamma(x)$:

$$\hat{b}_\Gamma(x) = \frac{1}{n}\sum_{i=1}^{n}\left[d_{O_i}(x) - d_{O_i^c}(x)\right], \quad x \in R^2$$

where $d_{O_i}(x)$ equals the Euclidean distance from x to the nearest pixel in the realization O_i, and $d_{O_i^c}(x)$ equals the Euclidean distance from x to the nearest pixel in the complement of O_i. Previous study showed that M_O has a denoising property in the sense that random speckles on an image can be averaged out (Jankowski and Stanberry, 2010). This property can smooth the details of sea ice boundary and leads to a too short length.

The Fréchet expectation M_H is based upon the Hausdorff distance ρ_H. ρ_H is equal to the greatest distance from a point in one set to the closest point in the other set. For two non-empty subsets A and B, their Hausdorff distance $\rho_H(A, B)$ is defined as:

$$\rho_H(A, B) = \max\left\{\max_{a\in A}\min_{b\in B} d(a, b),\ \max_{b\in B}\min_{a\in A} d(a, b)\right\}.$$

A realization O_i of Γ for which $E\left(\rho_H(\Gamma, O)^2\right)$ achieves its minimum is considered the Fréchet expectation. In our sea ice case, a daily sea ice extent that has a minimum square integrable Hausdorff distance compared with all the other daily ice extents in a month t is identified as M_H. Compared to the other four methods, M_H equals to a particular realization O_i. This may result in a very irregular shape of M_H including a great many details.

2.3. Trend calculation

For quantifying the trend, we first determined the 36-yr average for each calendar month; for the months of November and December, we used the 35-yr average. Second, the monthly deviations were generated by subtracting the 36- (or 35-) yr average from each individual monthly mean extent.

The linear regression model was fitted to the monthly deviation data. The slope of the fitting line indicated the trend in change and the standard error of the slope indicated the uncertainty range of the estimate. The slope was tested at the 0.001 and 0.01 significance level to identify whether the trend is statistically significant using the procedure in Parkinson et al. (1999) and subsequent works.

3. Results

3.1. Ice extent trends

The linear regression model was applied to monthly deviation data that were derived from all five averaging methods. We therefore obtained five different change rates for the period November 1978–December 2014. As an illustration, Fig. 1 presents plots of monthly sea ice extents and monthly deviations as derived from M_M. On average over the 36-yr period, the ice extent ranged from a minimum of 3.1×10^6 km^2 in February to a maximum of 19.5×10^6 km^2 in September, i.e., a maximum ice extent more than six times the minimum ice extent (Fig. 1(a) inset). After the seasonal cycle is removed, the existence of an upward trend becomes evident for each month with a statistically significant positive slope of $23.1 \pm 2.4 \times 10^3$ km^2 yr^{-1}.

The slopes for all five different methods are positive and statistically significant at the 99.9% confidence level. Except for M_H, the slopes of all the other four methods are similar, approximately 24×10^3 km^2 yr^{-1} with a standard error approximately equal to 2.3×10^3 km^2 yr^{-1}. M_H, however, has a flatter slope but it has the largest standard error, equal to $19.3 \pm 3.2 \times 10^3$ km^2 yr^{-1}.

To assess the influence of the observation years on the rates, we vary the endpoints of the calculation period from 1989 to 2014 (Fig. 2). Therefore, the first rate is for a decade from 1978 to 1989, and the last rate is for the entire 36-year period from 1978 to 2014. Generally, the five increasing trend lines are similar except for M_H. For endpoints before 1994, trend values in the Antarctic sea ice extent are negative. The trends turn positive only after 1995, and show a sharp growth after 2012 until reaching a value of approximately 24×10^3 km^2 yr^{-1}. From the 95% confidence band for M_H we observe that M_H has a significantly smaller positive trend than those derived from the other four methods after 1999.

3.2. Ice perimeter trends

Fig. 3 presents monthly average sea ice perimeters corresponding to the information that is presented in Fig. 1 for ice extent. The monthly mean perimeter (Fig. 3(a)) indicates a different basic seasonal cycle, ranging from 22.6×10^3 km in March to 42.3×10^3 km in December. After removing the seasonal cycle, the monthly deviations indicate noticeable differences for each of the five methods. M_M shows a slightly negative but statistically insignificant trend. M_A and M_O have positive trends at the 99% confidence level, at 20.8 ± 7.8 km yr^{-1} and 26.5 ± 5.6 km yr^{-1}, respectively. M_V and M_H have negative trends, with the two highest magnitudes -75.3 ± 11.1 km yr^{-1} and -71.5 ± 12.3 km yr^{-1}, respectively, at the 99.9% confidence level. Three monthly deviation curves were plotted in Fig. 3(b) as an illustration.

Unlike the extent trend shown in Fig. 2, the five methods indicate different time series trends for perimeters (Fig. 4). M_V and M_H show significant negative trends, with magnitudes that are consistently lower than the other methods for all the endpoints. M_A and M_O are in close agreement and remain positive after 1991. The year 1996 is a turning point: the trends vary rapidly prior to 1996, and keep stable after 1996. The trend line of M_M is located in the middle, with the narrow 95% confidence band not overlapping with any other lines. M_M shows a negative trend before 1996 and no obvious trend after 1996.

3.3. Special months

The five data sets of monthly averages were compared to their arithmetic mean (the mean of the five monthly average extents, denoted as M_{AA}) to determine the temporal structure of the difference. All the five methods showed significantly different ice extents as compared to M_{AA} by the

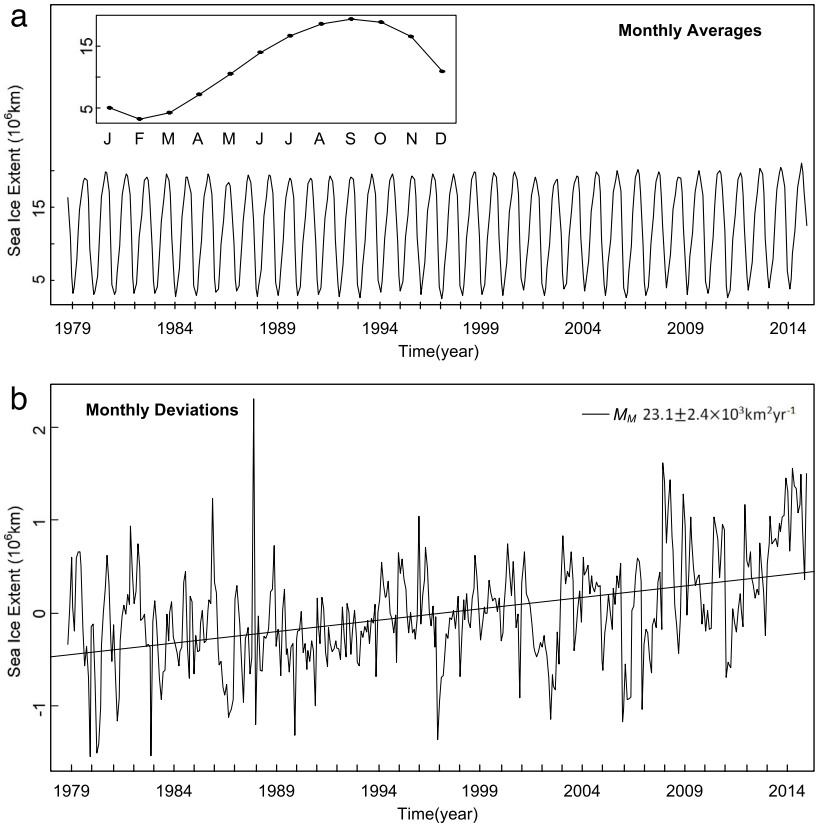

Fig. 1. (a) Monthly average Antarctic sea ice extents derived from M_M for November 1978 through December 2014, with an inset showing the average annual cycle. (b) Monthly deviations for the sea ice extents of part a, with the regression line and its slope and standard error.

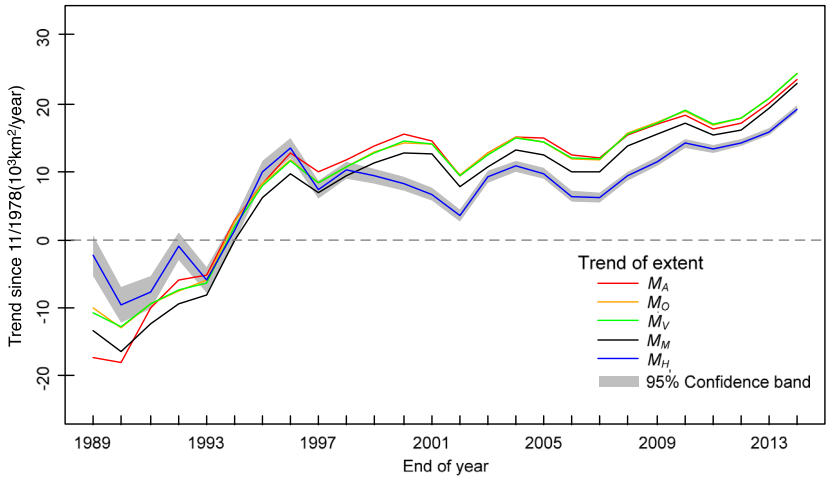

Fig. 2. Trends in the monthly-mean ice extent records at a range of endpoints.

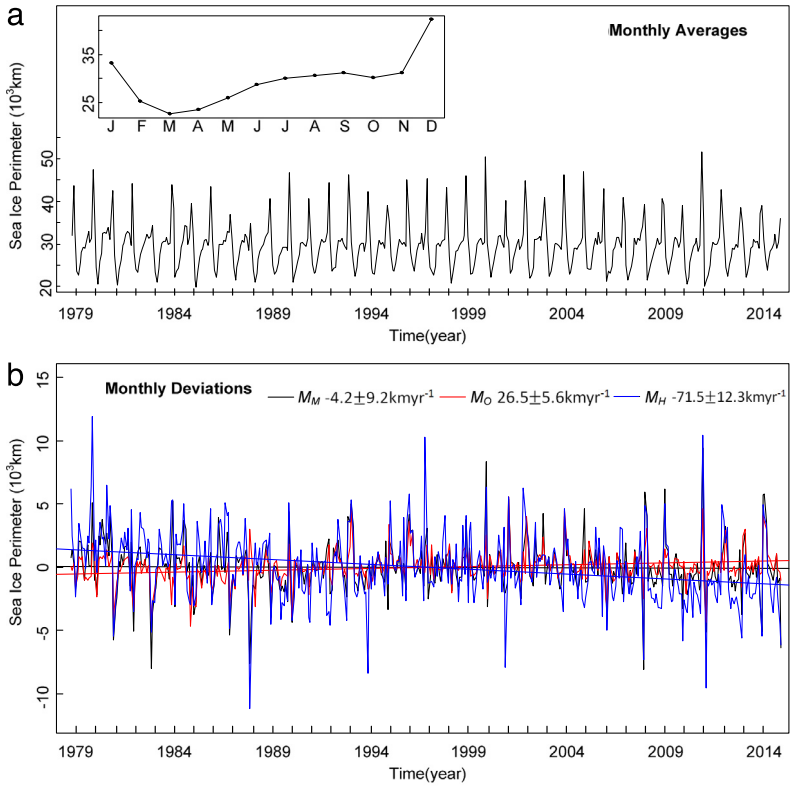

Fig. 3. (a) Monthly average Antarctic sea ice perimeters for November 1978 through December 2014, with an inset showing the average annual cycle. (b) Monthly deviations for the sea ice perimeters of part a, with the regression line and its slope and standard error.

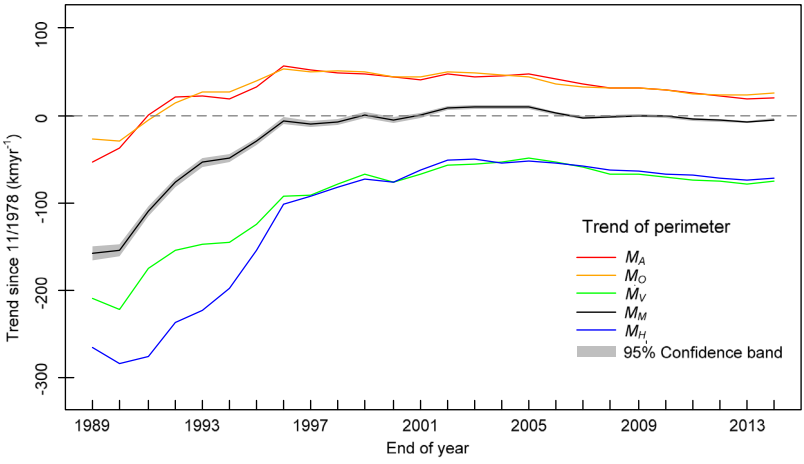

Fig. 4. Trends in the monthly-mean ice perimeter records at a range of endpoints.

Table 1
The maximum and minimum differences between five average methods and their mean.

Difference		$M_A - M_{AA}$	$M_O - M_{AA}$	$M_V - M_{AA}$	$M_M - M_{AA}$	$M_H - M_{AA}$
Extent (10^6 km^2)	Max	1.85	0.45	0.26	0.46	1.03
	Min	0	−0.63	−0.56	−0.64	−2.59
		$M_A - M_{AP}$	$M_O - M_{AP}$	$M_V - M_{AP}$	$M_M - M_{AP}$	$M_H - M_{AP}$
Perimeter (10^3 km)	Max	5	0.08	8.88	3.97	11.38
	Min	−7.14	−13.81	−1.18	−3.03	−1.21

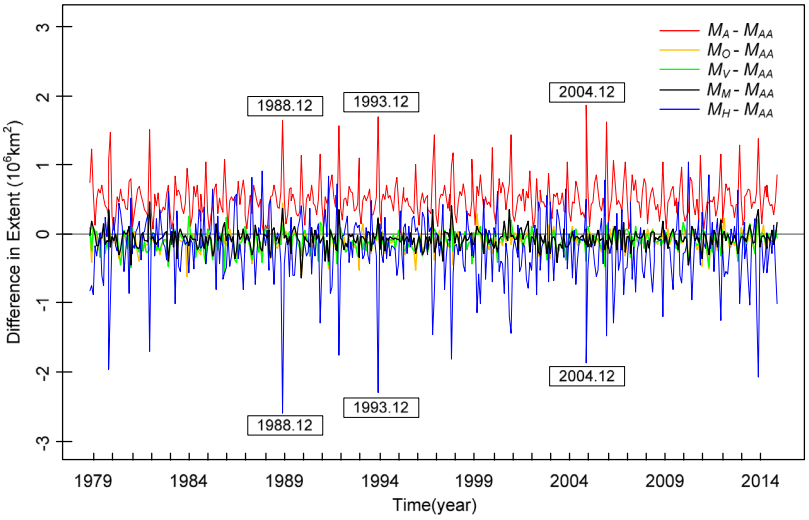

Fig. 5. Difference between monthly mean Antarctic sea ice extents computed using five average methods.

Friedman test. Among them, M_V agrees most closely with M_{AA}, in the range from -0.56×10^6 to 0.26×10^6 km^2 (Table 1). Higher extent estimates are provided by M_A, whereas M_H generally indicated lower extent estimates for most of the months, especially for December. The highest difference value (1.85×10^6 km^2) was recorded by M_A in Dec-2004, with values recorded in Dec-1988 and Dec-1993 almost reaching that level. The largest negative difference (-2.59×10^6 km^2) was recorded by M_H in Dec-1998, followed by Dec-1993. Apparently, December is a special month in which use of the five methods results in substantially different monthly extent estimations (see Fig. 5).

Fig. 6 presents a comparable display for Antarctic sea ice perimeters. The M_M perimeters are the only perimeters that are close to M_{Ap} (the average perimeter of the five monthly extents), with the narrowest range being -3.03×10^3 km to 3.97×10^3 km (Table 1). The M_H perimeters indicate substantial overestimations followed by the M_V perimeters, whereas the M_O perimeters indicate underestimations followed by the M_A perimeters. Like the ice extent, however, all five methods gave significantly different ice perimeters as compared to M_{Ap} by the Friedman test. The highest difference (11.38×10^3 km) was recorded by M_H in Nov-1996, with the difference reported for Dec-1979 almost reaching that level. The largest negative difference (-13.8×10^3 km) was recorded by M_O in Dec-1983, followed by Dec-1999 and Dec-2010. Consistent with what we found for monthly extent estimations, December is apparently a special month because use of the five methods resulted in monthly average extents with entirely different perimeters.

We grouped the daily sea ice extent and perimeter for each calendar month and plotted their statistical distributions as box plots (Fig. 7). The ice extents showed similar variations for all the months and indicated a maximum deviation in December. For perimeter estimation, however, there is a large variance indicated for the distances between whiskers on the boxes for each calendar month.

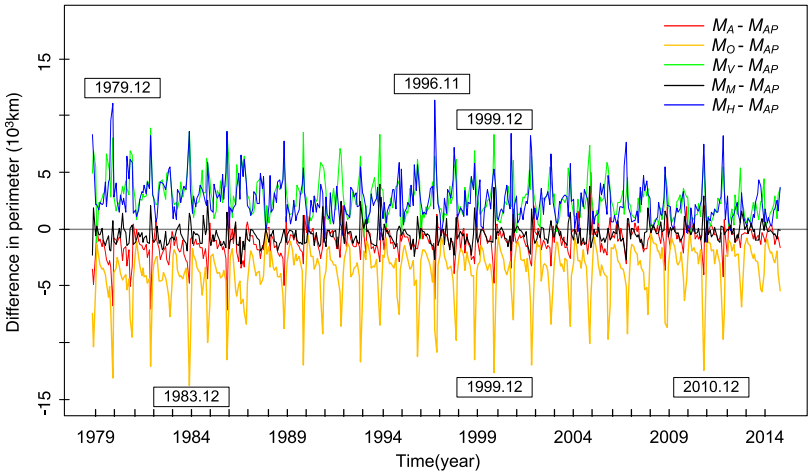

Fig. 6. Difference between monthly mean Antarctic sea ice perimeters computed using five average methods.

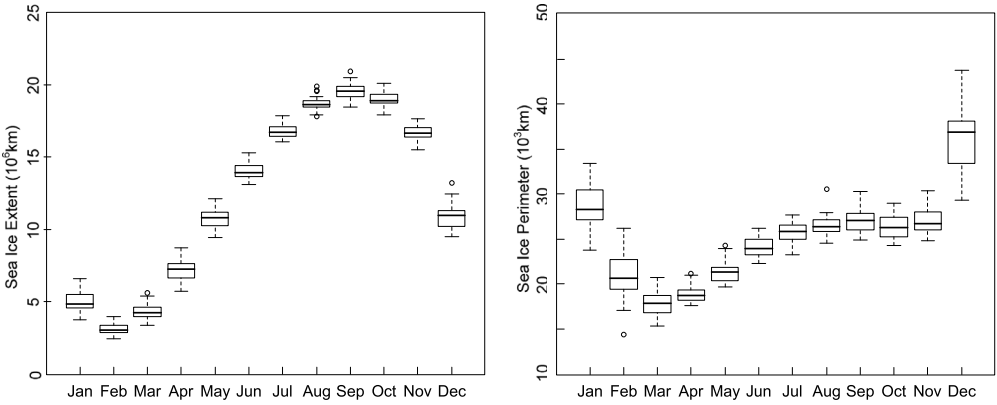

Fig. 7. Statistical distributions of monthly sea ice extents and perimeters.

For December, the lower whisker indicates a value that is only half of that of the upper whisker, which suggests a highly dynamic range for the daily perimeters for December. We therefore inferred that when the daily sea ice changes dramatically in one calendar month, it is easier to obtain different mean extents and perimeters.

Fig. 8 presents the five monthly mean ice extents overlaid on the covering function that displays the frequency of ice appearance in space. The extent of M_A is the most widely spread extent and has spatial coverage similar to the covering function. M_F indicates the smallest extent, which is only slightly larger than the core set of the covering function. The boundaries of M_V and M_M are in close agreement and represent the midrange of the monthly mean ice extents that were determined using the five averaging methods. M_O indicates similar extents as M_V and M_M but its boundary does not well coincide with the M_V and M_M boundaries.

Gaps among the monthly average boundaries often appear in the area where the covering function changes markedly. Based on the five-part Antarctic regional sectoring, the Weddell Sea and Indian Ocean have very different boundaries of the sea ice, followed by the Bellingshausen/Amundsen Seas (Fig. 8). The average ice extents in the Western Pacific Ocean and the Ross Sea were relatively more consistent. In the Weddell Sea and Indian Ocean, a irregular area of open water surrounded by sea ice, appears during a few days in Dec-2004, causing gradual changes in the covering function and most

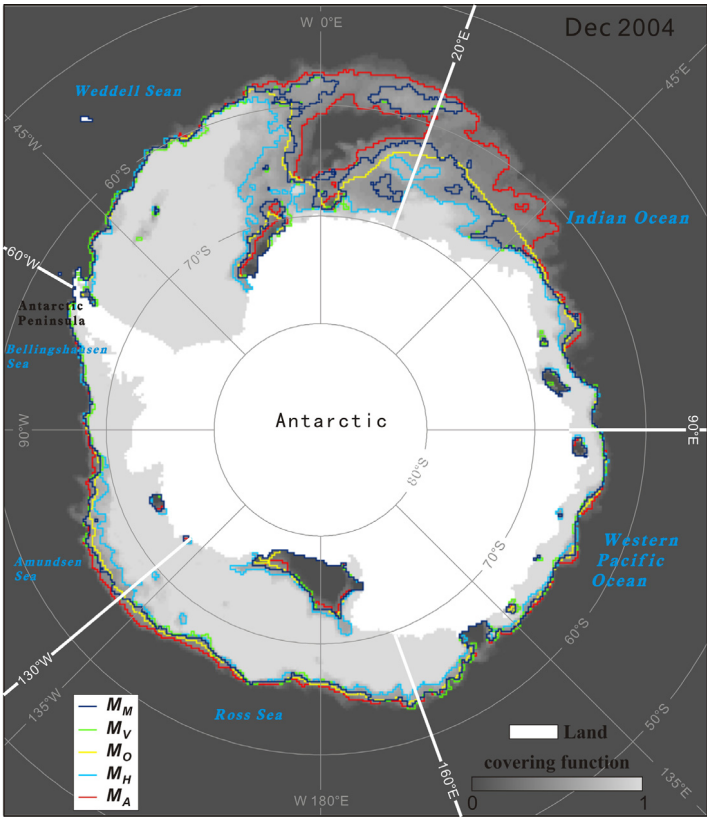

Fig. 8. Locations of the five monthly boundaries overlaid on the covering function of the Dec-2004.

of the gaps occur there. Another large open water exists in the Ross Sea during the entire month of December. This stable condition corresponds to a stable covering function and therefore results in more consistent monthly boundaries.

We checked the daily ice extent for Dec-2004 and confirmed that the daily ice extents spread over a large range of 14.1×10^6–7.1×10^6 km^2. This indicates that there is a large variance in the extent of the sea ice in Dec-2014, shrinking towards a half of its area in a single month. The biggest difference between the five mean extents can reach 3.7×10^6 km^2, which cannot be ignored by the users of the monthly December data.

4. Discussions

The upward trend of the sea ice extent is clearly indicated for the period November 1978–December 2014. Four out of five averaging methods provide statistically significant rates of approximately $24 \pm 2.3 \times 10^3$ km^2 yr^{-1}. This result has increased from the $17.1 \pm 2.3 \times 10^3$ km^2 yr^{-1} trend reported by Parkinson and Cavalieri (2012) for the monthly deviations for the period ending in December 2010, and even more from the $11.1 \pm 2.6 \times 10^3$ km^2 yr^{-1} trend for the shorter period ending in December 2006. We also observed this increasing trend from Fig. 2, which indicates that the positive rate has had a stable growth since 2007. Therefore, as the ending year was postponed and updated, we have additional proof regarding the growing trend of the Antarctic sea ice extent. In addition to the lengthening time span and associated addition of new data, including inconsistent source data and changes in the processing method may also cause changes in the trend. For example, Eisenman et al. (2014) found that the current Bootstrap Antarctic sea ice extent data set (Version 2) produced substantially

larger trends for a given time period than the Version 1 that was used prior to 2007. The accumulative effect of these uncertainties and error propagation in the process of calculating trend must be further studied in the future.

The comparison is reversed for the Antarctic sea ice perimeters. The trend in sea ice extent agrees closely among all the averaging methods, whereas the trend in sea ice perimeters differs substantially among the averaging methods for all time spans (Fig. 4). It is interesting to note that a transition occurred for all the methods in 1996. The difference between M_V and M_H diminished rapidly and all the methods maintained stable rates after 1996. This transition year coincides with the change in sensors in 1995 (Eisenman et al., 2014). Although some methods indicate positive trends and others indicate negative or non-significant trends, the magnitude of the rate is small as compared with the image resolution of 25 km. Furthermore, the length of the sea ice boundary measured on remote sensing images depends upon the image resolution. We therefore recommend that when reporting the trend in sea ice perimeters, the data source should be clarified and the averaging method that was applied in the evaluation of the monthly deviation should be specified.

Interestingly, ice extents and perimeters show different temporal patterns for different calendar months. The minimum monthly perimeter occurs in March, which is later than the smallest sea ice extent appearing in February. This inconsistency is caused by the shape of the ice boundary. Although in February the ice shrinks to its minimum range, the shapes of the ice boundaries are highly irregular. In March, when the sea ice first starts to expand but initially at a slow rate, the shape of ice outline becomes more convex and smooth, which results in a shorter perimeter than in February. The maximum monthly perimeter occurs in December rather than September, when the maximum extent appears. In addition to the shape factor, the occurrence of open water during the retreat and melt of ice plays an important role in December and January. According to the definition of perimeter in this study, the lengths of interior open water boundaries are included in the total perimeter calculation. As for the common features, the extent and perimeter both have their largest variability in December. Therefore, December is a special month that exhibits the most sensitivity to different averaging methods.

The spatial spread of monthly average ice extents can be determined with the use of random sets. A comparison of the five different averaging methods indicates that M_M is in close agreement with the mean of the five averaging methods and performs best in both extent and perimeter analysis. Moreover, M_M is a robust statistic that includes measurements in which extreme observations, e.g., daily ice extent outliers, have little effect on the monthly average result. M_M also has a physical meaning that the region is covered by sea ice for 50% of the time period. We therefore suggest M_M as a widely applicable method for the averaging process in studies on sea ice. M_V indicates a similar area size for the monthly extent and is calculated by arithmetically averaging daily ice extent in a conventional way. This makes the trend of M_V comparable with the rates of ice extent reported in previous publications. The advantage of M_V, however, is that its output is a geometric object instead of a single average value. We could know where the mean extent is located in space rather than its magnitude only. Because M_V indicates a substantially higher estimate for the perimeter, we put M_V at second place in our recommendation list of averaging methods. M_O performs well for estimating monthly extent. However, M_O shows definite underestimations for perimeters, which are probably caused by the smoothing effect resulting from its averaging process. As has been noted in Eisenman et al. (2014), M_A is likely to merge unexpected pixels into the ice edge, and thus overrates the ice extent. Among the five methods, only M_H takes a realization as its solution, whereas the others use the minimization process. In this case, M_H tends to have a more irregular shape, thus leading to a larger perimeter and unpredictable ice extents as compared to the other averaging methods. Moreover, computation of M_H is five times more time-consuming than the other averaging methods.

The sensitivity analysis performed in this paper is based on the comparison of five averaging methods. A reference on the "ground truth" is needed to determine which methods produce more accurate boundaries. Any reliable ground truth of monthly extents, however, does not exist in the real world. The sea ice extents change to a very low degree during a single day and a daily image only captures a snapshot of the ice state. The daily extents are integrated artificially to monthly average extents for the purpose of a trend analysis. Therefore, monthly mean extents resulting from integration depend upon the averaging method used in the processing and do not have an unambiguous true correspon-

dence with the situation in the real world. Even if images with a high spatial resolution would be used to extract the location of an ice edge, it is still impossible to validate the boundary of the monthly sea ice extent.

The gaps among sea ice boundaries derived from different methods, as shown in Fig. 8, tend to appear in the areas where the covering function changes rapidly. These areas usually occur where the sea ice retreats or expands continuously in space within several days in a month. For example, in December, formation of short-lived open water in the Weddell Sea and Indian Ocean and retreat of the ice edges in the Bellingshausen/Amundsen Seas correspond to large departures in the estimated mean extents. Because the Antarctic is a huge area (tens of millions of square kilometers), improved estimates can possibly be obtained if the sea ice boundary is studied locally in more detail (Zhao et al., 2015), e.g. at those areas where gaps occur. In addition to the month of December, other months that have large variations in daily extents and perimeters may also have distinct monthly averages, e.g., the months of April and May for the ice extent and the months of January and February for the perimeter.

5. Conclusions

In this paper, we investigated the variation of trends in the Antarctic sea ice extent and perimeter using five different averaging methods applied to daily data obtained from satellite images. Random sets were used to take uncertainties into account. The averaging methods provided a new perspective for determining the spatial location of the monthly mean ice extent rather than the conventional method, which only extracts a single value. Our results confirmed the statistically significant upward trend of Antarctic sea ice extent for the period November 1978–December 2014. The trends of the sea ice perimeter for the same period, however, were not consistent across the five different averaging methods. For all the other observation years, the trends of sea ice extent are more concentrated than those of the perimeter. In summary, the perimeter is more sensitive to the averaging methods. In addition, large gaps among monthly sea ice boundaries may occur in the regions where sea ice retreats or expands in a single month. We therefore should give more attention to estimations in the Weddell Sea and Indian Ocean, especially during the month of December, when the daily sea ice experience is more dynamic.

Acknowledgments

This work was partially supported by the National Natural Science Foundation of China (Grant Nos. 41301463 and 41576188). We thank two anonymous referees for their helpful comments.

References

Baddeley, A., Molchanov, I., 1998. Averaging of random sets based on their distance functions. J. Math. Imaging Vision 8, 79–92.
Cavalieri, D., Parkinson, C.L., 2008. Antarctic sea ice variability and trends, 1979–2006. J. Geophys. Res. 113.
Cavalieri, D., Parkinson, C.L., 2012. Arctic sea ice variability and trends, 1979–2010. Cryosphere 6, 881–889.
Cavalieri, D., Parkinson, C.L., DiGirolamo, N., Ivanoff, A., 2012. Intersensor calibration between F13 SSMI and F17 SSMIS for global sea ice data records. IEEE Geosci. Remote Sens. Lett. 9, 233–236.
Comiso, J.C., 2000. updated 2015. Bootstrap Sea Ice Concentrations from Nimbus-7 SMMR and DMSP SSM/I-SSMIS, Version 2. [1978.11-2014.12]. In http://dx.doi.org/10.5067/J6JQLS9EJ5HU Boulder, Colorado USA: NASA National Snow and Ice Data Center Distributed Active Archive Center.
Eisenman, I., Meier, W.N., Norris, J.R., 2014. A spurious jump in the satellite record: has Antarctic sea ice expansion been overestimated? Cryosphere 8, 1289–1296.
Friel, N., Molchanov, I.S., 1999. A new thresholding technique based on random sets. Pattern Recognit. 32, 1507–1517.
IPCC. 2007. Climate Change 2007: The Physical Science Basis. In: Solomon, S., Qin, D., Manning, M., Chen, Z., Marquis, M., Averyt, K.B., Tignor, M., Miller, H.L. (Eds.), Contribution of Working Group I to the Fourth Assessment Report of the Intergovernmental Panel on Climate Change, Cambridge, United Kingdom, New York, NY, USA.
IPCC. 2013. Climate Change 2013: The Physical Science Basis. In: Stocker, T.F., Qin, D., Plattner, G.-K., Tignor, M., Allen, S.K., Boschung, J., Nauels, A., Xia, Y., Bex, V., Midgley, P.M. (Eds.), Contribution of Working Group I to the Fifth Assessment Report of the Intergovernmental Panel on Climate Change, Cambridge, United Kingdom, New York, NY, USA.
Ivanova, N., Pedersen, L.T., Tonboe, R.T., Kern, S., Heygster, G., Lavergne, T., Sørensen, A., Saldo, R., Dybkjær, G., Brucker, L., Shokr, M., 2015. Satellite passive microwave measurements of sea ice concentration: an optimal algorithm and challenges. Cryosphere Discuss. 9, 1269–1313.

Jankowski, H., Stanberry, L.I., 2010. Expectations of random sets and their boundaries using oriented distance functions. J. Math. Imaging Vision 36, 291–303.
Massom, R.A., Stammerjohn, S.E., 2010. Antarctic sea ice change and variability—Physical and ecological implications. Polar Sci. 4, 149–186.
Molchanov, I.S., 1998. Averaging of random sets and binary images. CWI Q. 11, 371–384.
Molchanov, I.S., 2005. Random closed sets. In: Bilodeau, M., Meyer, F., Schmitt, M. (Eds.), Space, Structure, and Randomness. pp. 135–149.
Parkinson, C.L., Cavalieri, D., 2012. Antarctic sea ice variability and trends, 1979–2010. Cryosphere 6, 871–880.
Parkinson, C.L., Cavalieri, D., Gloersen, P., Zwally, H.J., Comiso, J.C., 1999. Arctic sea ice extents, areas, and trends, 1978–1996. J. Geophys. Res. 104, 20837–20856.
Simmonds, I., 2015. Comparing and contrasting the behaviour of Arctic and Antarctic sea ice over the 35 year period 1979–2013. Ann. Glaciol. 56, 18–28.
Stoyan, D., 1997. Set-valued means of random particles. J. Math. Imaging Vis. 7, 111–121.
Stoyan, D., Stoyan, H., 1994. Fractals, Random Shapes and Point Fields. Wiley, Chichester.
Vorob'ov, O.Y., 1996. Random set models of fire spread. Fire Technol. 32, 137–173.
Worby, A.P., Comiso, J.C., 2004. Studies of the Antarctic sea ice edge and ice extent from satellite and ship observations. Remote Sens. Environ. 92, 98–111.
Zhao, X., Stein, A., Chen, X., 2010. Application of random sets to model uncertainties of natural entities extracted from remote sensing images. Stoch. Environ. Res. Risk Assess. 24, 713–723.
Zhao, X., Su, H., Stein, A., Pang, X., 2015. Comparison between AMSR-E ASI sea-ice concentration product, MODIS and pseudo-ship observations of the Antarctic sea-ice edge. Ann. Glaciol. 56, 45–52.
Zhou, L., 2014. Areal uncertainty in traffic island polygons extracted from airborne laser point clouds. In: Faculty of Geo-Information and Earth Observation (ITC). University of Twente, Enschede.